




Article

Development of Alumina–Mesoporous Organosilica Hybrid Materials for Carbon Dioxide Adsorption at 25 °C

Chamila Gunathilake ^{1,2}, Rohan S. Dassanayake ³, Chandrakantha S. Kalpage ¹ and Mietek Jaroniec ^{2,*}

¹ Department of Chemical and Processing Engineering, Faculty of Engineering, University of Peradeniya, Peradeniya 20400, Sri Lanka; chamilag@pdn.ac.lk (C.G.); csk@eng.pdn.ac.lk (C.S.K.)

² Department of Chemistry and Biochemistry, Kent State University, Kent, OH 44242, USA

³ Department of Chemistry, Ithaca College, Ithaca, NY 14850, USA; rdassanayake@ithaca.edu

* Correspondence: jaroniec@kent.edu; Tel.: +1-330-672-3790

Received: 27 September 2018; Accepted: 13 November 2018; Published: 16 November 2018



Abstract: Two series of alumina (Al₂O₃)–mesoporous organosilica (Al–MO) hybrid materials were synthesized using the co-condensation method in the presence of Pluronic 123 triblock copolymer. The first series of Al–MO samples was prepared using aluminum nitrate nanahydrate (Al–NN) and aluminum isopropoxide (Al–IP) as alumina precursors, and organosilanes with three different bridging groups, namely tris[3-(trimethoxysilyl)propyl]isocyanurate, 1,4-bis(triethoxysilyl)benzene, and bis(triethoxysilyl)ethane. The second series was obtained using the aforementioned precursors in the presence of an amine-containing 3-aminopropyltriethoxysilane to introduce, also, hanging groups. The Al–IP-derived mesostructures in the first series showed the well-developed porosity and high specific surface area, as compared to the corresponding mesostructures prepared in the second series with 3-aminopropyltriethoxysilane. The materials obtained from Al–NN alumina precursor possessed enlarged mesopores in the range of 3–17 nm, whereas the materials synthesized from Al–IP alumina precursor displayed relatively low pore widths in the range of 5–7 nm. The Al–IP-derived materials showed high CO₂ uptakes, due to the enhanced surface area and microporosity in comparison to those observed for the samples of the second series with AP hanging groups. The Al–NN- and Al–IP-derived samples exhibited the CO₂ uptakes in the range of 0.73–1.72 and 1.66–2.64 mmol/g at 1 atm pressure whereas, at the same pressure, the Al–NN and Al–IP-derived samples with 3-aminopropyl hanging groups showed the CO₂ uptakes in the range of 0.72–1.51 and 1.70–2.33 mmol/g, respectively. These data illustrate that Al–MO hybrid materials are potential adsorbents for large-scale CO₂ capture at 25 °C.

Keywords: alumina; CO₂ capture; porous hybrid adsorbents; mesoporous organosilica

1. Introduction

Among many heat-trapping gases, including CO₂, SO₂, NO, N₂O, NO₂, and CH₄, carbon dioxide (CO₂) is considered one of the major contributors to global warming. According to the report released by EPA in 2011, the contribution of CO₂ is about 84% of the total discharge of gases into the atmosphere. Currently, the CO₂ concentration exceeded 400 ppm, and the average global temperature has already increased by 1–2 °C, as compared to the values reported over the last few decades. Although this temperature fluctuation seems to be small, it has a significant effect on the global climate patterns, leading to the melting of glaciers in north and south poles, eventually causing the sea level to rise. Thus, reducing the concentration level of CO₂ is an urgent requirement to keep the atmosphere safe and diminish the effects of global warming.

Nowadays, the preferred technology for industrial CO₂ capture involves chemical absorption in aqueous solutions of amines. Alkanolamines, including monoethanolamine (MEA) and diethanolamine (DEA), are commonly used in this process [1]. However, the amine-based scrubbing techniques possess several drawbacks. For instance, the regeneration of absorbed CO₂ from liquid amine is energy intensive, and replacement of amine after several cycles is needed due to its degradation under oxidizing and reducing chemical environments.

Solid sorbents have attracted a great attention as potential alternatives to the liquid amine scrubbing techniques, due to their high stability, tunability, and reusability. Unlike aqueous liquid amines, porous solid sorbents adsorb CO₂ via physisorption (physical adsorption) [2] or chemisorption (chemical adsorption) [2], and avoid many drawbacks associated with liquid amines [3,4]. Chemisorption on solid sorbents is achieved by modifying their surface with basic sites such as alkaline carbonates and different amine functional groups, which show high affinity toward acidic CO₂. Physical solid sorbents for CO₂ capture include activated carbons [5,6], carbon molecular sieves [7,8], carbon nanotube-based sorbents [9,10], zeolites [11,12], and metal-organic frameworks [13,14]. Materials like alkali metal-based sorbents [15–18], amine-functionalized solid sorbents such as activated carbons [19,20], carbon nanotubes [21,22], solid resins [23], modified zeolite-based sorbents [24,25], polymer-based sorbents [26,27], amine-functionalized silica [28,29], grafted silica sorbents [30–32], and amine-impregnated alumina sorbents [33], have been investigated as chemical solid sorbents.

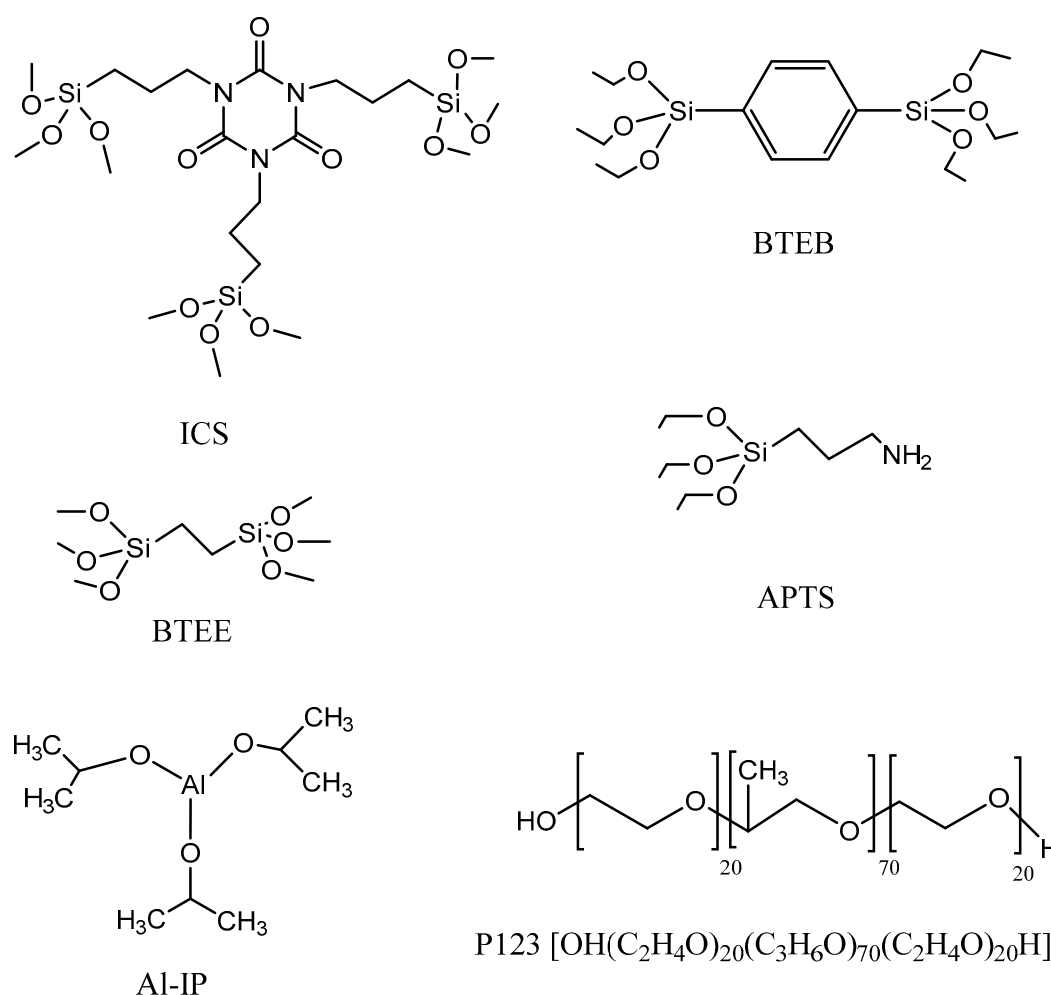
Mesoporous silica materials, such as SBA-15 [34] and MCM-41 [35], have been investigated for CO₂ capture. However, these materials show low CO₂ sorption capacities due to weak interactions between silanol groups and CO₂. Therefore, MCM-41 and SBA-15 silica materials modified with different amine groups, including diethylenetriamine, tetraethylenepentamine, polyethyleneimine, and ethylenediamine, have been studied for CO₂ capture [30–32,36–40]. The chemical incorporation of amine groups onto silica matrix can be achieved either by co-condensation [41,42] or post-synthesis grafting [31,43,44]. Typically, the higher loading of amine groups leads to higher CO₂ capacity depending on the properties of mesoporous silica. Thus, the selection of proper silica support with high porosity and high surface area before amine grafting is essential. During grafting of amine groups onto silica surface, the surface silanols react with aminosilanes. Therefore, maintaining high surface silanol density is beneficial for achieving higher loading of amine groups and larger CO₂ sorption capacity.

Over the past few years, the amine-grafted mesoporous silica and impregnated alumina materials have been investigated as solid sorbents for CO₂ capture [45,46]. Mesoporous silica inherits high surface area, tunable, and well-defined porosity, which are important for uniform grafting of amine functional groups. Similarly, alumina materials show favorable properties, including high surface area, high porosity, and thermal and mechanical stability, which are suitable for amine modification. The adsorption properties of alumina strongly depend on its structure and thermal treatment temperature (calcination temperature). For example, mesoporous alumina materials feature large pore volume, three-dimensional (3D) interconnected mesoporosity, and thermal stability. Due to these unique characteristics, alumina-based materials have been investigated for gas adsorption applications. Examples of alumina-based materials for CO₂ capture include amine-impregnated Al₂O₃ [33], basic Al₂O₃ [46], amine-modified mesoporous Al₂O₃ [47,48], MgO/Al₂O₃ [49], and Al₂O₃–organosilica [50] materials.

Interestingly, the adsorption properties of alumina–mesoporous silica composites can be further improved by introducing silica precursors with nitrogen-containing functional groups, such as amines and organic bridging groups [50,51]. We previously reported the synthesis of alumina–mesoporous organosilica hybrid materials with isocyanurate bridging groups and their CO₂ adsorption properties at elevated temperatures [50]. Incorporation of organic bridging groups facilitated the formation of crosslinked mesostructures with well-ordered pores and enhanced surface properties [51]. In addition,

the organic moieties of bridging groups increase hydrophobicity of the mesoporous silica matrix, which is beneficial for CO₂ sorption.

In this study, we report the synthesis and CO₂ adsorption properties of mesoporous Al–MO hybrid materials at 25 °C. Here, we also present the effects of different alumina precursors, silica precursors with varying organic bridging groups, amine-based silica hanging groups, and calcination process on the CO₂ capture at 25 °C. Al–MO hybrid materials were prepared in the presence of triblock copolymer Pluronic P123 using alumina and organosilica precursors. Two alumina precursors used in this study include aluminum nitrate nanahydrate (Al–NN) and aluminum isopropoxide (Al–IP), see Scheme 1. Silanes with three different bridging groups, including nitrogen-containing tris[3-(trimethoxysilyl)propyl]isocyanurate (ICS), and non-nitrogen-containing 1,4-bis(triethoxysilyl)benzene (BTEB), and bis(triethoxysilyl)ethane (BTEE)), were used as organosilica precursors. The grafting of amine groups was achieved by using 3-aminopropyltriethoxysilane (APTS), see Scheme 1. To our knowledge, this is the first report on the Al–MO hybrid materials prepared by using different alumina and silica precursors with various organic bridging groups and amine hanging groups for CO₂ capture at ambient conditions.



Scheme 1. Structures of the chemicals used in the synthesis of different Al–MO hybrid materials.

2. Materials and Methods

2.1. Materials

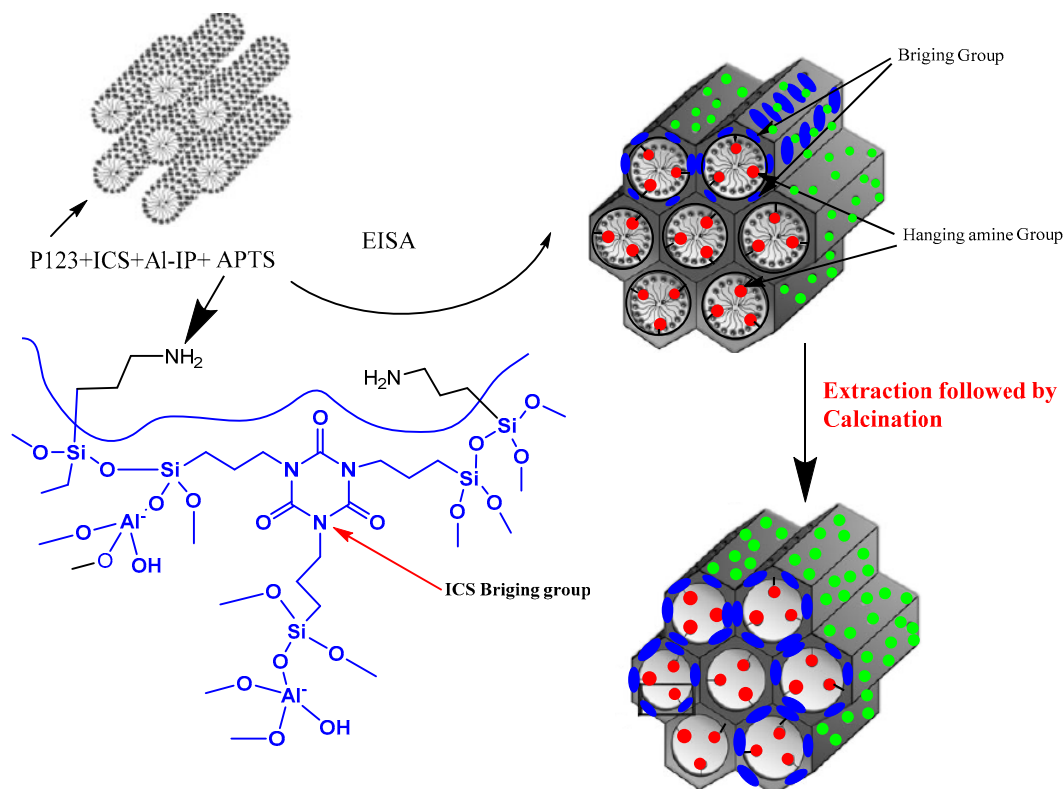
Tris[3-(trimethoxysilyl)propyl]isocyanurate (ICS), 1,4-bis(triethoxysilyl)benzene (BTEB), bis(triethoxysilyl)ethane (BTEE), and 3-aminopropyltriethoxysilane (APTS) were purchased from

Gelest Inc (Morrisville, PA, USA). Pluronic P123 (EO₂₀PO₇₀EO₂₀) triblock copolymer was purchased from BASF Corporation (Florham Park, NJ, USA). Absolute ethanol was obtained from AAPER Alcohol and Chemical Company (Shelbyville, KY, USA). Ethanol (95%) was purchased from Fisher Scientific (Pittsburgh, PA, USA). Aluminum isopropoxide (Al-IP) and aluminum nitrate nanahydrate (Al-NN) were purchased from Sigma Aldrich (St. Louis, MO, USA). All reagents were in analytical grade, and used without further purification.

2.2. Synthesis Method

Alumina-mesoporous organosilica (Al-MO) hybrid samples were synthesized using a slightly modified literature method [50,52]. The procedure used for the preparation of the first series of Al-MO hybrid materials was as follows: 1.0 g of Pluronic P123 (EO₂₀PO₇₀EO₂₀) and known amounts of Al-NN (aluminum nitrate nanahydrate) or Al-IP (aluminum isopropoxide) were added to 20 mL of absolute ethanol in a 250 mL polypropylene bottle. Then, the reaction mixture was stirred at 25 °C for 70 min. After that, a predetermined amount of silica precursor with different organic bridging groups (ICS, BTEE or BTEB) was added to the resultant mixture. The same steps were used in the preparation of the second series of Al-MO hybrid materials with APTS hanging groups. A known amount of APTS was added to the reaction mixture after adding the silica precursor (ICS, BTEE, or BTEB). In both cases, the final mixture was stirred at room temperature for 4 h and kept in an oven at 60 °C for 48 h. Then, extraction of the P123 block copolymer template from the resulting white/yellow solid was performed using 55 mL of 95 % ethanol solution in a 250 mL polypropylene bottle under vigorous stirring for a few minutes. The resulting dispersion was kept in the oven (Sheldon Manufacturing Inc., Cornelius, OR, USA) at 100 °C for another 24 h. Next, the product was filtered and rinsed thoroughly with 95 % ethanol and dried in an oven at 70 °C for an additional 20 h. Finally, calcination of the solid obtained after extraction was conducted in a horizontal quartz tube furnace (Lindberg Blue M manufactured by Thermal Product Solutions, White Deer, PA, USA) at 350 °C for 2 h in flowing N₂ at a heating rate of 2 °C/min. The samples obtained prior to the extraction step (as-synthesized), after extraction (extracted), and after extraction followed by calcination (extracted and calcined), were tested for their adsorption properties. Scheme 2 shows the route used for the synthesis of alumina-organosilica (Al-IC10-AP10) material using two organosilanes, the first with an isocyanurate bridging group (ICS) and the second with 3-aminopropyl (APTS) hanging group.

The aluminum content (0.011 mol) was kept constant for all samples studied. The number of moles of Si used in the synthesis was a percentage of the total number of Al moles. Based on our previous study, the optimum Si% for tris[3-(trimethoxysilyl)propyl]isocyanurate (ICS) and 3-aminopropyltriethoxysilane (APTS) was found to be 10% [50]. The Al-MO materials with higher Si% than 10 showed smaller pore widths due to the geometrical constraints created by bulky silane bridging groups during self-assembly process [50]. Therefore, Si percentage, with respect to the total number of Al moles, was maintained at 10% for all Al-MO samples. The samples were denoted based on the precursors used in the initial reaction mixture. For instance, the short abbreviation AN refers to aluminum nitrate nanahydrate (Al-NN), and AI to aluminum isopropoxide (Al-IP). Short abbreviations IC, B, E, and AP, were used for tris[3-(trimethoxysilyl)propyl]isocyanurate (ICS), 1,4-bis(triethoxysilyl)benzene (BTEB), bis(triethoxysilyl)ethane (BTEE), and 3-aminopropyltriethoxysilane (APTS), respectively. For instance, AN-B10 refers to the samples synthesized using Al-NN and BTEB (10% Si), whereas AN-B10-AP10 refers to the samples synthesized using Al-NN, and BTEB (10% Si) and APTS (10% Si). In both cases, Al-NN acts as an alumina precursor. Similarly, AI-B10 refers to the samples prepared using Al-IP and BTEB (10% Si), while AI-B10-AP10 refers to the samples obtained by using Al-IP, BTEB (10% Si), and APTS (10% Si). The as-synthesized samples are denoted with a # mark. Labels for all extracted samples do not have an asterisk (*), whereas the samples subjected to the extraction, followed by calcination, are marked with an asterisk (*).



Scheme 2. Illustration of the synthesis route for alumina–organosilica material (Al-IC10-AP10) using isocyanurate bridging silane (ICS) and 3-aminopropyltriethoxysilane (APTS).

Four analogous samples to AN-IC10, AN-IC10*, AN-IC10-AP10, and AN-IC10-AP10* were studied in a previous work [50], where a series of materials was prepared by varying the amount of ICS. The synthesis and calcination conditions used in [50] and this work are slightly different, which results in different adsorption parameters. For instance, AN-IC10 in the current paper was calcined at 350 °C with heating rate of 2 °C/min, while an analogous sample reported in [50] was calcined at 300 °C with heating rate of 3 °C/min. In previous work [50], alumina precursors were mixed with one bridging silane only, isocyanurate (IC), by varying its percentage from 10 to 80%, while, in this work, silanes (10% only) with different bridging were explored. Importantly, the previous work [50] was focused on the CO₂ capture at elevated temperatures, while the current work reports the newly synthesized samples with different functional groups for CO₂ adsorption at 25 °C.

2.3. Characterization of Materials

Nitrogen (N₂) adsorption isotherms were collected at −196 °C (77 K) using an ASAP 2010 volumetric analyzer (Micromeritics, Inc., Norcross, GA, USA). All materials were outgassed under vacuum at 110 °C for 2 h before recording the adsorption measurements.

High-resolution thermogravimetric measurements were conducted using a TGA Q-500 analyzer (TA Instruments, Inc., New Castle, DE, USA). Thermogravimetric (TG) studies were performed from 25 °C to 700 °C in flowing N₂ gas, using a heating rate of 10 °C/min. The TG profiles were used to study the thermal stability of the hybrid materials and the removal of P123 template.

2.4. NMR Analysis

All NMR spectra were collected on Bruker Avance (III) 400WB NMR spectrometer (Bruker Biospin Corporation, Billerica, MA, USA) equipped with a magic-angle spinning (MAS) triple resonance probe head having zirconia rotors of 4 mm diameter by using the procedure reported in [50].

2.5. CO₂ Adsorption Measurements

CO₂ adsorption studies were conducted using an ASAP 2020 volumetric adsorption analyzer (Micromeritics, Inc., Norcross, GA, USA) at the pressures up to ~1.2 atm and 25 °C using ultrahigh pure CO₂ gas. All samples were outgassed at 110 °C for 2 h under vacuum before the analysis. The sample reusability was tested over a number of adsorption/desorption cycles for the sample with the highest CO₂ adsorption capacity. Six consecutive adsorption/desorption runs were recorded on ASAP 2020. For instance, the first adsorption isotherm measurement was carried out up to 1.2 atm followed by desorption cycle. After the completion of the first run, the second adsorption/desorption run was started manually on the same instrument, and so on.

2.6. Calculation of Surface Properties

The Brunauer–Emmett–Teller (BET) specific surface area (S_{BET}) of each sample was calculated by following its N₂ adsorption isotherm in the relative pressure range of 0.05 to 0.20. The single-point pore volume (V_{sp}) was determined based on the amount N₂ gas adsorbed at a relative pressure of ~0.98. The pore size distributions (PSD) were calculated using adsorption branches of N₂ adsorption/desorption isotherms and applying the improved Kruk–Jaroniec–Sayari (KJS) method developed for cylindrical pores [53]. The total pore volume (V_{t}) was calculated by integrating the entire PSD curve and the volume of micropores (V_{mi}) was calculated by taking the difference between V_{t} and V_{meso} ($V_{\text{t}} - V_{\text{meso}}$). The mesopore volume (V_{meso}) was determined by integrating the PSD curve from 2 nm to the end of the PSD curve. In addition to the PSD curves that display the overall distribution of pores, the pore widths (W_{max}) corresponding to the maxima of these distributions are also tabulated to show the characteristic pore sizes of the samples studied.

3. Results and Discussion

3.1. Properties of Al–MO Hybrid Composites

High-resolution thermogravimetry (HR-TG) and differential thermogravimetry (DTG) studies were conducted to identify the thermal stability of silica precursors with ethylene, benzene, isocyanurate bridging groups, and amine hanging groups. Figure 1 shows the DTG profiles recorded in flowing N₂ for AN-IC10[#], AN-IC10*, and AN-IC10-AP10* samples. As shown in Figure 1, all samples exhibit a sharp peak approximately at 100 °C, assigned to the loss of physically adsorbed water. The as-synthesized (AN-IC10[#]) sample displays two additional peaks on its DTG profile in the temperature ranges of 150–300 °C and 350–480 °C, corresponding to the decomposition of P123 block copolymer template and isocyanurate bridging groups, respectively, see Figure 1.

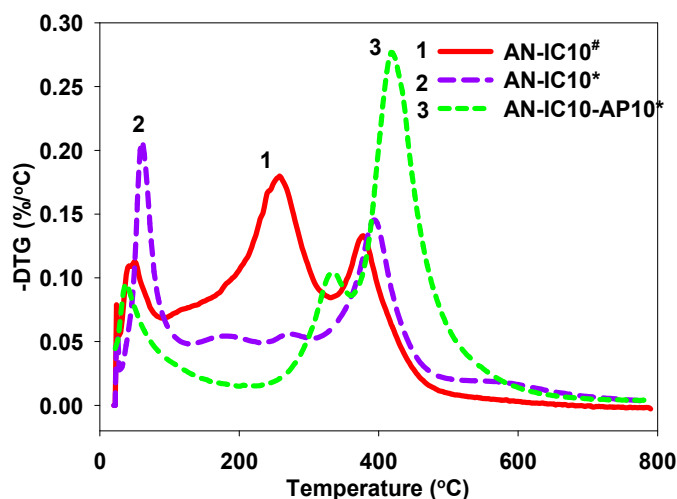


Figure 1. DTG profiles of the as-synthesized ([#]) alumina–silica composite with isocyanurate bridging groups and alumina–silica composites with isocyanurate bridging groups in the presence and absence of aminopropyl groups after extraction followed by calcination (*). Note: AN and AP refer to the aluminum nitrate and aminopropyl, respectively.

The DTG profiles obtained for the extracted and calcined alumina–silica samples (AN-IC10-AP10* and AN-IC10*) with isocyanurate (ICS) bridging groups in the presence and absence of aminopropyl group show a second major peak centered at 430 °C, related to the decomposition of isocyanurate bridging groups, see Figure 1. The small peak observed at 330 °C for AN-IC10-AP10* corresponds to the degradation of aminopropyl groups. The DTG profiles for AN-IC10-AP10* and AN-IC10* do not have any peak in the temperature range from 150 to 300 °C, indicating the complete removal of block copolymer template via extraction followed by calcination, see Figure 1. The corresponding TG curves of AN-IC10[#], AN-IC10*, and AN-IC10-AP10* samples are shown in Figure 2. Figure 3 displays the DTG profiles of three extracted and calcined alumina–silica samples (AN-IC10*, AN-E10*, and AN-B10*) with ICS, BTEE, and BTEB bridging groups. As can be seen from Figure 3, peaks at ~400, 550, and 600 °C correspond to the thermal degradation of isocyanurate, benzene, and ethylene bridging groups, respectively.

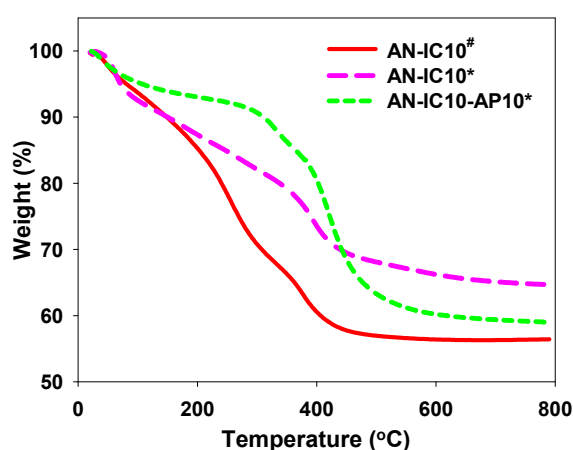


Figure 2. TG profiles of the as-synthesized ([#]) alumina–silica sample with isocyanurate bridging groups and alumina–silica samples with isocyanurate bridging groups in the presence and absence of aminopropyl groups after the extraction and calcination (*). Note that AN and AP refer to the aluminum nitrate and aminopropyl, respectively.

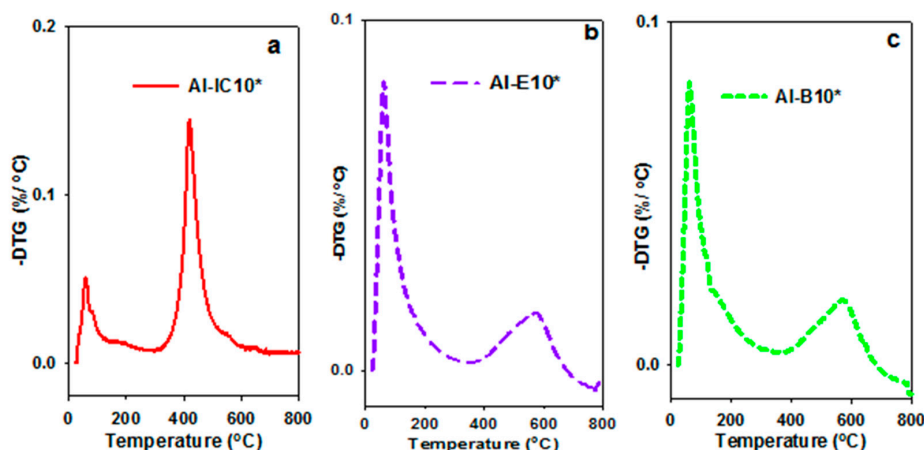


Figure 3. DTG profiles for the extracted and calcined (*) alumina–silica composites containing isocyanurate (IC; panel a), ethylene (E; panel b), and benzene (B; panel c) bridging groups. Note that Al refers to aluminum isopropoxide.

Figures 4 and 5 show comparisons of N_2 adsorption/desorption isotherms for the Al–MO samples synthesized using Al–NN as an alumina precursor with three different bridged organosilanes in the absence and presence of 3-aminopropyltriethoxysilane (AP) at $-196\text{ }^\circ\text{C}$ (77 K), respectively. All extracted (AN-B10, AN-E10, AN-IC10, AN-B10-AP10, AN-E10-AP10, AN-IC10-AP10), and extracted and calcined (AN-B10*, AN-E10*, AN-IC10*, AN-B10-AP10*, AN-E10-AP10*, AN-IC10-AP10*) samples exhibit type IV nitrogen adsorption isotherms with steep capillary condensation–evaporation steps beginning at a relative pressure of around 0.85 (see adsorption isotherms in Figures 4 and 5). Insets in Figures 4 and 5 show the pore size distribution (PSD) curves corresponding to the aforementioned adsorption isotherms obtained by the KJS method [53]. Our N_2 adsorption isotherms reveal that the extracted samples derived from Al–NN (AN-IC10, AN-B10, AN-E10, AN-B10-AP10, AN-E10-AP10) have better surface properties, as evidenced by higher surface area, total pore volume (V_t), and pore width (W_{max}), as compared to the extracted and calcined counterparts (AN-IC10*, AN-B10*, AN-E10*, AN-B10-AP10*, AN-E10-AP10*). This may be attributed to the shrinkage of organosilica structure due to the calcination process at a relatively high temperature ($350\text{ }^\circ\text{C}$) [54].

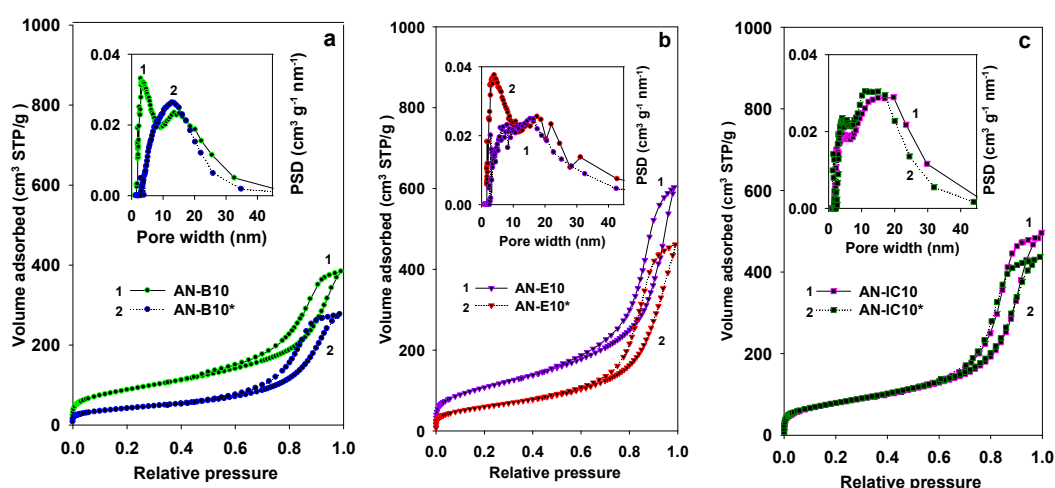


Figure 4. N_2 adsorption isotherms and their corresponding PSD curves (insets) for the extracted (AN-B10 (left panel a), AN-E10 (middle panel b), and AN-IC10 (right panel c)), and extracted and calcined (AN-B10* (left panel a), AN-E10* (middle panel b), and AN-IC10* (right panel c)) samples. AN refers to aluminum nitrate.

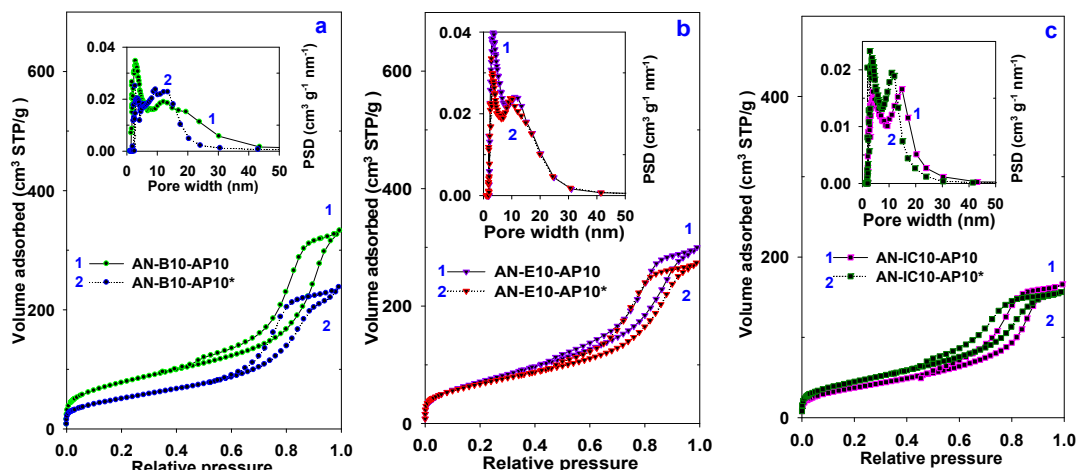


Figure 5. N_2 adsorption isotherms and their corresponding PSD curves (insets) for extracted (AN-B10-AP10 (left panel a), AN-E10-AP10 (middle panel b), and AN-IC10-AP10 (right panel c)), and extracted calcined (AN-B10-AP10* (left panel a), AN-E10-AP10* (middle panel b), and AN-IC10-AP10* (right panel c)) samples. Note that AN and AP refer to aluminum nitrate and aminopropyl, respectively.

Similar to the Al-NN-derived samples, all Al-IP-derived samples also show type IV isotherm with relatively broad capillary condensation–evaporation steps pertained to H1 type hysteresis loop (see Figures 6 and 7) and quite narrow PSDs (see insets in Figures 6 and 7). As shown in Table 1, all extracted and calcined samples derived from Al-IP (AI-B10*, AI-E10*, AI-IC10*, AI-B10-AP10*, AI-E10-AP10*, and AI-IC10-AP10*) exhibit lower surface parameters, including surface area, microporosity, and pore width, as compared to the corresponding extracted samples (AI-B10, AI-E10, AI-IC10, AI-B10-AP10, AI-E10-AP10, and AI-IC10-AP10). For example, the specific surface area of AI-IC10 decreases from $655\text{ m}^2\cdot\text{g}^{-1}$ to $618\text{ m}^2\cdot\text{g}^{-1}$ after grafting aminopropyl hanging groups (AI-IC10-AP10*). In addition, the pore width of AI-IC10 sample reduces from 5.6 nm to 5.4 nm after introducing aminopropyl hanging groups (AI-IC10-AP10*), see Table 1. The reduction in the surface properties of the extracted and calcined samples is due to the shrinkage of the organosilica structure upon calcination at $350\text{ }^\circ\text{C}$ [54].

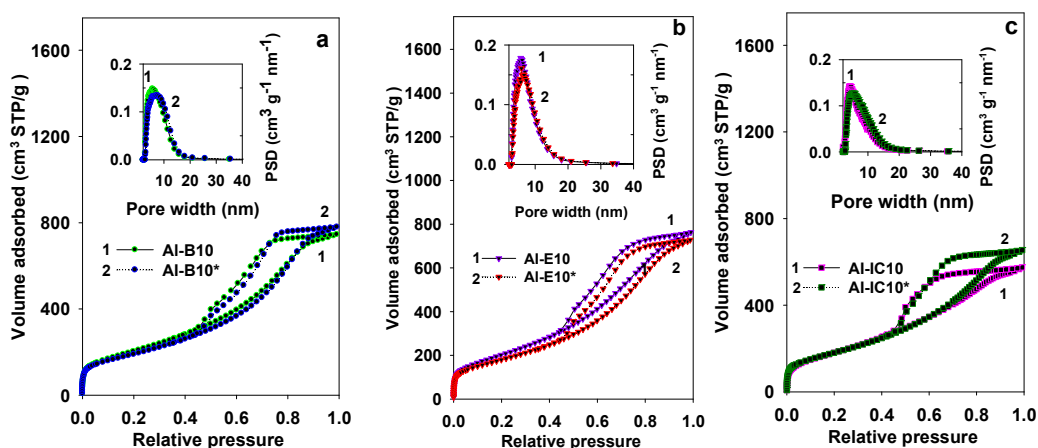


Figure 6. N_2 adsorption isotherms and their respective PSD curves (insets) for the extracted (AI-B10 (left panel a), AI-E10 (middle panel b), and AI-IC10 (right panel c)), and extracted calcined (AI-B10* (left panel a), AI-E10* (middle panel b), AI-IC10* (right panel c)) samples, where B, E, and IC refer to benzene, ethylene, and isocyanurate bridging groups, respectively; AI refers to aluminum isopropoxide.

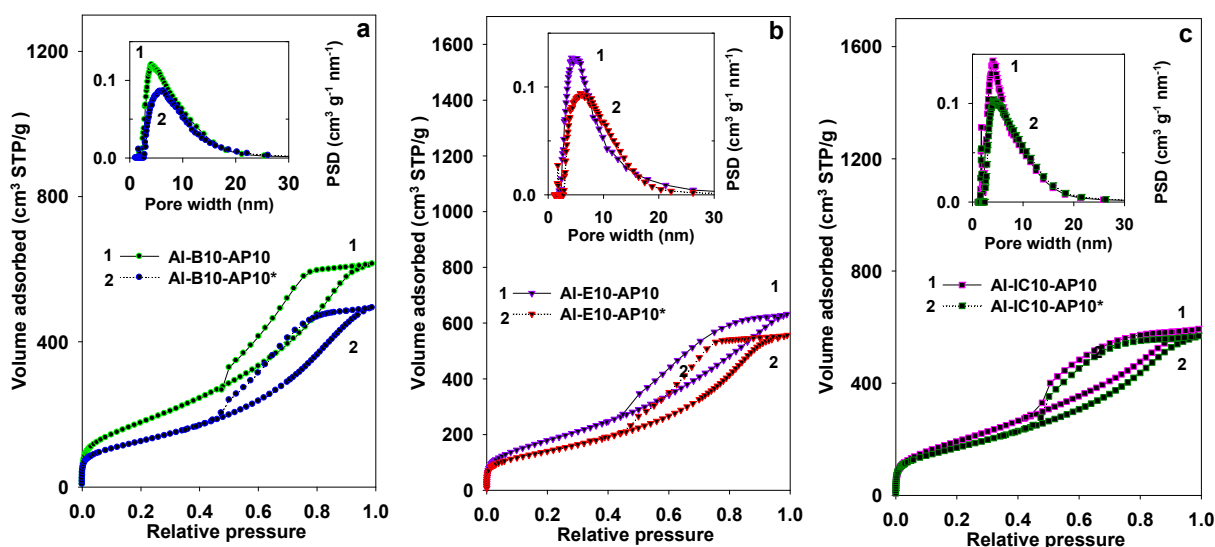


Figure 7. N_2 adsorption isotherms (left panel) and the corresponding PSD curves (insets) for the extracted (AI-B10-AP10 (left panel a), AI-E10-AP10 (middle panel b), and AI-IC10-AP10 (right panel c)), and extracted calcined (AI-B10-AP10* (left panel a), AI-E10-AP10* (middle panel b), AI-IC10-AP10* (right panel c)) samples. AI refers to aluminum isopropoxide, and AP represents aminopropyl.

Table 1. Adsorption parameters obtained for the alumina–silica samples studied.

Samples	S_{BET} (m^2/g)	V_{sp} (cc/g)	V_t (cc/g)	V_{mi} (cc/g)	W_{max} (nm)	n_{CO_2} (mmol/g)	$n^*_{CO_2}$ ($\mu mol/m^2$)
AN-B10	319	0.60	0.63	0.02	2.9/13.6	0.78	2.45
AN-B10*	150	0.42	0.44	<0.01	12.0 [#]	0.73	4.87
AN-E10	393	0.91	0.94	<0.01	4.1/17.0	1.09	2.77
AN-E10*	219	0.67	0.72	<0.01	15.9 [#]	0.85	3.88
AN-IC10	289	0.74	0.77	0.01	4.0/16.4 [#]	0.92	3.18
AN-IC10*	286	0.68	0.68	<0.01	4.0/13.2 [#]	1.72	6.01
AN-B10-AP10	284	0.50	0.52	0.02	2.9/12.3	0.96	3.38
AN-B10-AP10*	186	0.36	0.38	<0.01	9.4/13.3	1.22	6.56
AN-E10-AP10	265	0.46	0.48	<0.01	3.4/11.6 [#]	0.74	2.79
AN-E10-AP10*	247	0.42	0.43	<0.01	3.2/9.8 [#]	1.51	6.11
AN-IC10-AP10	138	0.26	0.26	<0.01	4.1/14.8	0.72	5.21
AN-IC10-AP10*	163	0.24	0.24	<0.01	3.6/11.1	1.40	8.59
AI-B10	742	1.14	1.24	0.05	5.1	2.60	3.50
AI-B10*	684	1.20	1.28	0.03	6.1	1.99	2.91
AI-E10	740	1.18	1.27	0.03	5.7	2.64	3.57
AI-E10*	652	1.12	1.19	0.02	6.1	2.35	3.60
AI-IC10	664	0.89	0.95	0.04	4.1	1.66	2.50
AI-IC10*	655	1.01	1.06	0.02	4.7	2.39	3.65
AI-B10-AP10	654	0.94	1.00	0.02	4.2	1.83	2.80
AI-B10-AP10*	452	0.76	0.78	<0.01	5.6	1.74	3.85
AI-E10-AP10	664	0.97	1.03	0.02	4.0	1.86	2.80
AI-E10-AP10*	509	0.86	0.90	<0.01	5.1	1.70	3.34
AI-IC10-AP10	713	0.91	0.98	0.03	4.0	2.33	3.27
AI-IC10-AP10*	618	0.87	0.90	0.02	5.4	2.21	3.58

S_{BET} —specific surface area, V_{sp} —single point pore volume, V_t —total pore volume, V_{mi} —volume of micropores, W_{max} —pore width ([#] refers to the middle value of the “flat” PSD peak), n_{CO_2} —number of moles of CO_2 adsorbed at 1 atm per gram of the sample, and $n^*_{CO_2}$ —number of moles of CO_2 adsorbed at 1 atm per unit surface area of the sample. B, E, or IC refer to benzene, ethylene, and isocyanurate bridging groups, respectively; AN and AP refer to aluminum nitrate and aminopropyl, respectively. Extracted, and extracted and calcined samples, are denoted without* and with*, respectively.

It is noteworthy that the samples prepared from Al–IP precursor show much higher surface area and total pore volume (V_t) as compared to the analogous samples prepared from Al–NN precursor,

see Table 1 and Figure 7. For instance, the specific surface area of AI-B10 is $742 \text{ m}^2 \cdot \text{g}^{-1}$, as compared to $319 \text{ m}^2 \cdot \text{g}^{-1}$ of AN-B10, and the total pore volume (V_t) of AI-B10 is $1.24 \text{ cm}^3 \cdot \text{g}^{-1}$ as compared to $0.63 \text{ cm}^3 \cdot \text{g}^{-1}$ of AN-B10, see Table 1. However, AI-NN-derived samples exhibit higher pore widths as compared to AI-IP-derived samples. For example, the pore width of AN-B10 sample is 13.6 nm as compared to 5.6 nm of AI-B10 sample.

^{13}C , ^{27}Al , and ^{29}Si solid-state NMR spectra provide a comprehensive description of the chemical environment of carbon, aluminum, and silicon atoms present in the AI-MO materials studied. For instance, ^1H - ^{29}Si cross polarization (CP) MAS NMR spectra reflect the degree of condensation of the siloxane bonds of isocyanurate, benzene, ethylene bridging groups, and aminopropyl hanging groups present in the hybrid organosilica framework. ^{27}Al magic-angle spinning (MAS) NMR spectra reveal the coordination of the incorporated aluminum units in the AI-MO composites. ^1H - ^{13}C CP/MAS NMR spectra confirm the presence of organic bridging (B, E, IC) and surface aminopropyl groups. The ^{27}Al MAS NMR spectra exhibit three peaks for the AI-MO samples studied, see Figure 8. As shown in Figure 8, both AI-IC10* and AN-IC10* samples display an intense resonance peak at 3.7 ppm attributed to the aluminum species in an octahedral environment. The additional weak resonance peaks, visible at about 66.8 and 34.5 ppm, can be attributed to the aluminum in tetrahedral and pentahedral symmetries, respectively. The ^1H - ^{29}Si CP/MAS NMR spectra of the AI-B10*, AI-E10*, and AI-IC10* samples show one prominent resonance peak at -82.2 ppm (Figure 9), corresponding to Q^2 ($\text{Si}-(\text{OSi})_2(\text{OH})_2$)/($\text{Si}-(\text{OSi})_2(\text{OH})(\text{OAl})$) groups. The spectrum of AI-E10* displays an additional small peak at ~ -47 ppm, corresponding to the T^1 ($\text{R}-\text{Si}-(\text{OSi})_1(\text{OH})_2$) structure. There are no visible peaks above 90 ppm, indicating the absence of Q^n ($n = 3,4$) structures. Figure 10 shows the ^1H - ^{13}C CP/MAS spectra of the AI-IC10-AP10*, AI-B10-AP10*, and AI-E10-AP10* samples. The AI-IC10-AP10* and AI-B10-AP10* samples show three characteristic resonance peaks at 9, 21, and 44 ppm, referring to the carbon atoms bonded to Si atoms, carbon atoms present in the middle of propyl chain, and carbon atoms directly attached to N atoms, respectively. The characteristic sharp peaks at 150 and 138 ppm reflect carbon atoms in isocyanurate and benzene bridging groups, respectively. The spectrum of the AI-E10-AP10* sample exhibits four distinct peaks at 5.5, 9.0, 21.0, and 28.9 ppm. The first peak at 5.5 ppm refers to ethylene bridging groups. The second peak at 9 ppm refers to the carbon atoms present in the aminopropyl chain directly bonded to silicon. Note that the carbon atom directly bonded to Si also appears at 9 ppm. The third and fourth peaks at 21 and 28 ppm, of AI-E10-AP10* sample, correspond to the carbon atoms in the middle of the propyl chain and carbon atoms directly attached to N atoms in the aminopropyl chain, see Figure 10.

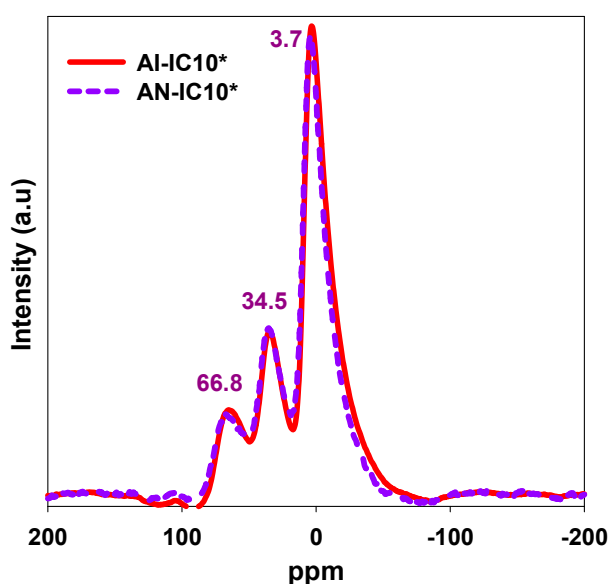


Figure 8. ^{27}Al -MAS NMR spectra of the AI-IC10* and AN-IC10* for extracted and calcined samples.

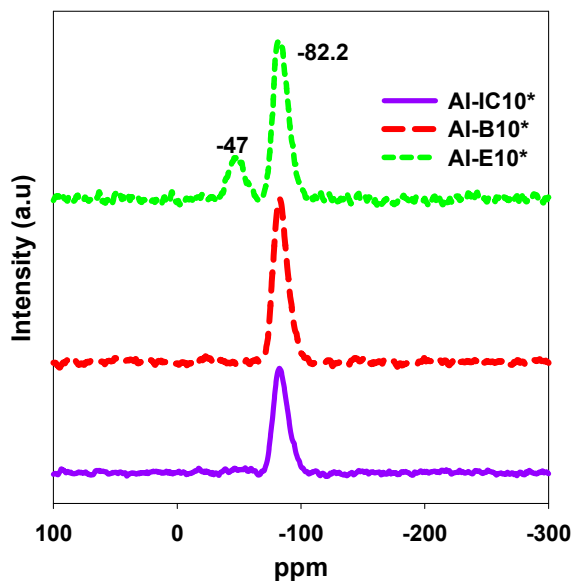


Figure 9. ^1H - ^{29}Si -MAS NMR spectra of the AI-IC10*, AI-B10*, and AI-E10* samples.

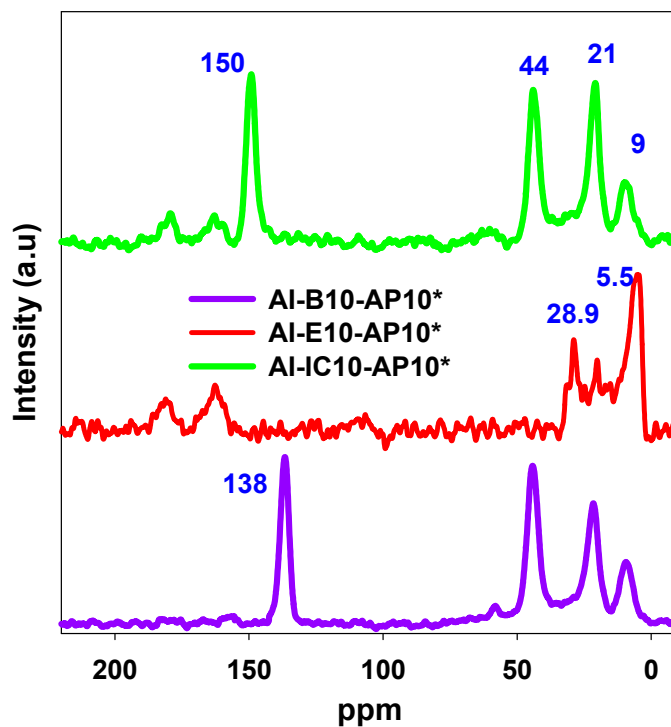


Figure 10. ^1H - ^{13}C CP/MAS NMR spectra of the AI-IC10-AP10*, AI-E10-AP10*, and AI-B10-AP10* samples.

3.2. CO_2 Sorption

Four series of Al-MO samples were examined for CO_2 adsorption at pressures up to ~ 1.2 atm and 25°C . Figures 11 and 12 show a comparison of CO_2 adsorption isotherms measured for all Al-MO samples studied. AN-B10, AN-E10, and AN-IC10 samples, and their extracted-followed-by-calcination counterparts (AN-B10*, AN-E10*, and AN-IC10*) show CO_2 uptakes at 1 atm in the range from 0.72 to 1.72 mmol/g (Table 1 and Figure 11a). However, AI-B10, AI-E10, and AI-IC10 samples, and their extracted-followed-by-calcination counterparts (AI-B10*, AI-E10*, and AI-IC10*) exhibit higher CO_2 uptakes at 1 atm, varying from 1.66 to 2.64 mmol/g (Table 1 and Figure 12a).

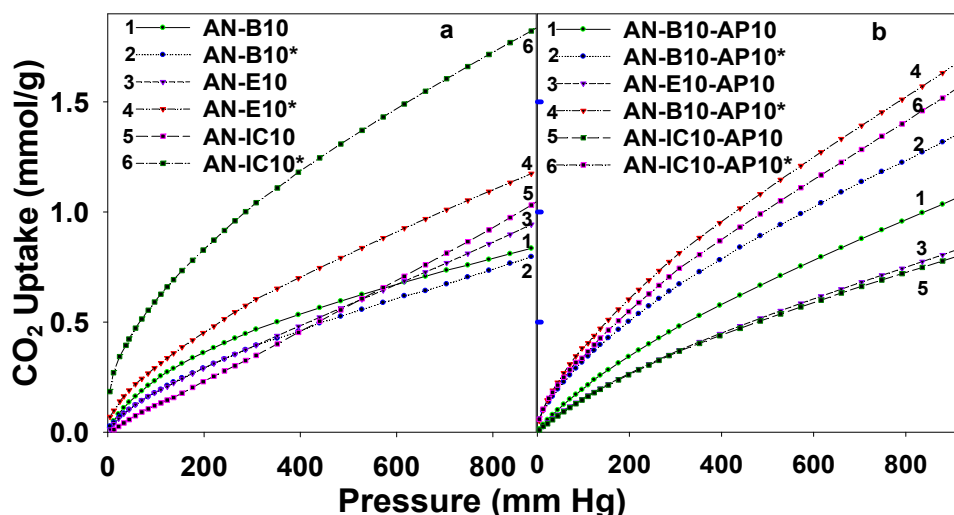


Figure 11. CO₂ adsorption profiles at 25 °C, measured on the extracted, and extracted and calcined a) AN-Z10 and b) AN-Z10-AP10 samples, where Z = B, E, or IC.

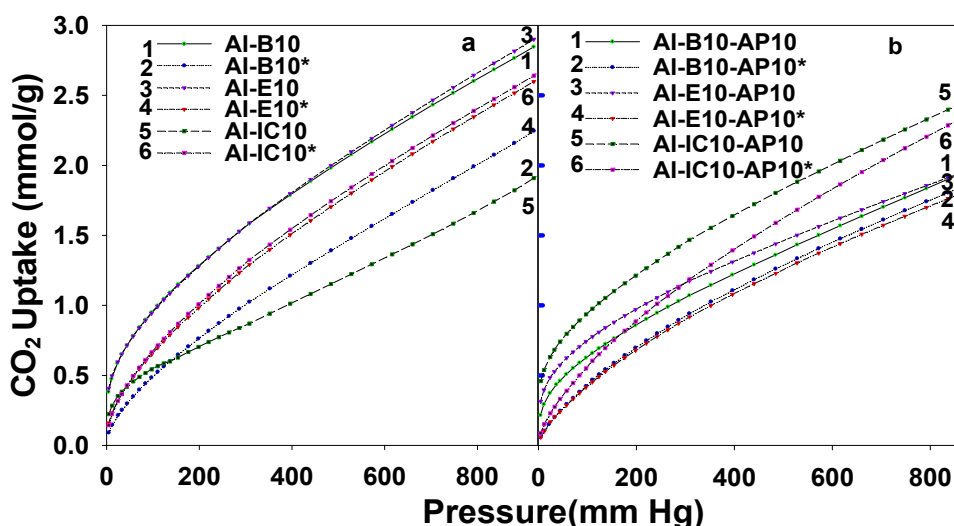


Figure 12. CO₂ adsorption profiles at 25 °C measured on the extracted, and extracted and calcined (*) (a) AN-Z10 and (b) AN-Z10-AP10 samples, where Z = B, E, or IC.

It has been previously reported that the CO₂ adsorption at ambient temperature is governed by a physisorption mechanism, which is dependent on the volume of micropores (below 2 nm), in particular, ultramicropores (below 0.7 nm) and surface area [55,56]. However, the samples studied show very low micropore volumes, suggesting that, in this case, the surface area and surface properties are major factors determining the CO₂ adsorption (see Table 1). Moreover, the samples synthesized using Al-IP precursor show an approximately two-fold increase in the specific surface area and microporosity, in comparison to the corresponding samples synthesized from Al-NN precursor (see Table 1) and, consequently, their CO₂ uptakes at 1 atm are higher. Our results also reveal that the structure of alumina precursor plays a vital role in determining the surface properties of the Al-MO hybrid materials. Therefore, aluminum isopropoxide (Al-IP) precursor works better than aluminum nitrate nanahydrate (Al-NN) precursor, due to its ability to form 3D extended mesoporous structures with block copolymers during the co-condensation process [54,57]. Among three silica precursors, organosilica composite with ethylene groups (Al-E10) exhibits the highest CO₂ uptake of 2.64 mmol/g at 1 atm, see Table 1. At the same pressure, the samples with benzene (Al-B10) and isocyanurate (Al-IC10*) bridging groups exhibit the CO₂ uptakes of 2.60 and 2.39 mmol/g, respectively. Our data suggest that the samples subjected to extraction and calcination have lower surface parameters, including microporosity, mesoporosity,

surface area, and pore size (see Table 1), as compared to the samples subjected to extraction only, which is due to the shrinkage of the Al–MO materials at high temperatures. For example, the extracted and calcined samples with benzene and ethylene bridging groups show slightly lower CO₂ adsorption capacities as compared to the samples subjected to extraction only. The CO₂ uptakes measured at 1 atm for Al–B10 and Al–E10 change from 2.60 and 2.64 mmol/g, to 1.99 and 2.35 mmol/g, when calcination is performed (see Table 1). By contrast, the CO₂ uptakes measured for the extracted and calcined samples with nitrogen-containing isocyanurate group (AN–IC10* and AI–IC10*) are larger than those for the extracted samples (AN–IC10 and AI–IC10), see Table 1. Higher CO₂ adsorption on the AN–IC10* and AI–IC10* samples could be assigned to the unique structure of isocyanurate group and the presence of nitrogen species favoring interactions with CO₂. Grafting aminopropyl hanging groups on the surface of the Al–MO composites did not cause a significant effect on the CO₂ uptake (see Table 1). Al–MO samples with aminopropyl hanging groups also display lower microporosity and surface area (see Table 1 and Figures 11 and 12). Our results demonstrate that the CO₂ adsorption on mesoporous alumina–organosilica materials is mainly determined by the surface area of the sample, alumina precursor, and structure and functionality of the organic bridging groups. Calcination of the alumina–silica samples at 350 °C did not improve their adsorption properties. Amine-containing materials are commonly used as chemical sorbents at higher temperatures; however, grafting amine groups on the Al–MO materials did not affect physisorption of CO₂ at the conditions studied.

Cycle stability of the Al–MO material with the highest CO₂ adsorption capacity was also tested as described previously [58,59]. Cycle stability measurements for Al–E10 were conducted for six consecutive cycles, and CO₂ uptake was measured. The CO₂ uptake remained stable after six adsorption/desorption cycles with approximately 2.64 mmol/g CO₂ uptake at 1 atm, suggesting good stability of Al–E10 materials. Note that the alumina samples (extracted and calcined at 350 °C) do not show a long-range order on the XRD profiles; thus, they are amorphous in nature (data not shown).

Alumina-based composite materials have been investigated for CO₂ capture. Table 2 summarizes a comparison of CO₂ uptakes for various alumina-based composite materials reported in the literature at low and elevated temperatures. However, studies of alumina-based materials for CO₂ capture at ambient conditions are rare. The sorbents studied in this work show much higher CO₂ uptake at 25 °C, as compared to the values reported previously for alumina-based materials under the same conditions.

Table 2. Comparison of the CO₂ sorption data for different alumina-based composite materials.

Material	Temperature (°C)	Pressure (atm)	CO ₂ Uptake (mmol/g)	Ref.
Al–Mg oxide	60 (13%H ₂ O)	0.99	1.36	[49]
Al ₂ O ₃ –silica	120	0.99	2.20	[50]
Al–Zr–mixed oxide–silica	0	1	1.83	[58]
	25	1	1.39	
	60	1	2.60	
	120	1	2.37	
Al–Mg mixed oxide–silica	300	0.99	0.46	[60]
γ–Al ₂ O ₃	60	9.9	1.94	[61]
N-doped γ–Al ₂ O ₃	55	NG	0.67	[62]
Al–Mg mixed oxide–nitrate–graphene oxide	60	1	1.00	[63]
Al ₂ O ₃ –silica	25	1	2.64	This work

4. Conclusions

Mesoporous alumina–organosilica (Al–MO) materials exhibited high CO₂ adsorption capacity at 25 °C. CO₂ adsorption properties of Al–MO materials depend on the surface area of the sample,

alumina precursor, and structure and functionality of the organosilica bridging group. The Al–NN- and Al–IP-derived samples exhibited the highest CO₂ uptakes of 1.72 and 2.64 mmol/g at 1 atm, respectively. High CO₂ uptake, reusability, selectivity, and good thermal and mechanical stability, make Al–MO materials potential adsorbents for larger-scale CO₂ capture at 25 °C.

Author Contributions: Writing—Review & Editing, C.G, R.S.D, C.S.K, M.J.

Funding: This research received no external funding.

Acknowledgments: Authors thanks to Mahinda Gangoda for technical support with NMR measurements.

Conflicts of Interest: The authors declare no conflict of interest.

References

1. Dassanayake, R.S.; Gunathilake, C.; Dassanayake, A.C.; Abidi, N.; Jaroniec, M. Amidoxime-functionalized nanocrystalline cellulose–mesoporous silica composites for carbon dioxide sorption at ambient and elevated temperatures. *J. Mater. Chem. A* **2017**, *5*, 7462–7473. [[CrossRef](#)]
2. Burwell, R.L. Section 1—Definitions and Terminology. In *Manual of Symbols and Terminology for Physicochemical Quantities and Units—Appendix II*; Burwell, R.L., Ed.; Pergamon Press: Oxford, UK, 1976; pp. 74–86.
3. Oschatz, M.; Antonietti, M. A search for selectivity to enable CO₂ capture with porous adsorbents. *Energy Environ. Sci.* **2018**, *11*, 57–70. [[CrossRef](#)]
4. Nugent, P.; Belmabkhout, Y.; Burd, S.D.; Cairns, A.J.; Luebke, R.; Forrest, K.; Pham, T.; Ma, S.; Space, B.; Wojtas, L.; et al. Porous materials with optimal adsorption thermodynamics and kinetics for CO₂ separation. *Nature* **2013**, *495*, 80–84. [[CrossRef](#)] [[PubMed](#)]
5. Dong, F.; Lou, H.; Goto, M.; Hirose, T. A new PSA process as an extension of the Petlyuk distillation concept. *Sep. Purif. Technol.* **1999**, *15*, 31–40. [[CrossRef](#)]
6. Kikkinides, E.S.; Yang, R.T.; Cho, S.H. Concentration and recovery of carbon dioxide from flue gas by pressure swing adsorption. *Ind. Eng. Chem. Res.* **1993**, *32*, 2714–2720. [[CrossRef](#)]
7. Burchell, T.D.; Judkins, R.R.; Rogers, M.R.; Williams, A.M. A novel process and material for the separation of carbon dioxide and hydrogen sulfide gas mixtures. *Carbon* **1997**, *35*, 1279–1294. [[CrossRef](#)]
8. Rutherford, S.W.; Do, D.D. Adsorption dynamics of carbon dioxide on a carbon molecular sieve 5A. *Carbon* **2000**, *38*, 1339–1350. [[CrossRef](#)]
9. Cinke, M.; Li, J.; Bauschlicher, C.W.; Ricca, A.; Meyyappan, M. CO₂ adsorption in single-walled carbon nanotubes. *Chem. Phys. Lett.* **2003**, *376*, 761–766. [[CrossRef](#)]
10. Huang, L.; Zhang, L.; Shao, Q.; Lu, L.; Lu, X.; Jiang, S.; Shen, W. Simulations of Binary Mixture Adsorption of Carbon Dioxide and Methane in Carbon Nanotubes: Temperature, Pressure, and Pore Size Effects. *J. Phys. Chem. C* **2007**, *111*, 11912–11920. [[CrossRef](#)]
11. Inui, T.; Okugawa, Y.; Yasuda, M. Relationship between properties of various zeolites and their carbon dioxide adsorption behaviors in pressure swing adsorption operation. *Ind. Eng. Chem. Res.* **1988**, *27*, 1103–1109. [[CrossRef](#)]
12. Siriwardane, R.V.; Shen, M.-S.; Fisher, E.P. Adsorption of CO₂, N₂, and O₂ on Natural Zeolites. *Energy Fuels* **2003**, *17*, 571–576. [[CrossRef](#)]
13. Demessence, A.; D’Alessandro, D.M.; Foo, M.L.; Long, J.R. Strong CO₂ Binding in a Water-Stable, Triazolate-Bridged Metal–Organic Framework Functionalized with Ethylenediamine. *J. Am. Chem. Soc.* **2009**, *131*, 8784–8786. [[CrossRef](#)] [[PubMed](#)]
14. Yazaydin, A.Ö.; Snurr, R.Q.; Park, T.-H.; Koh, K.; Liu, J.; LeVan, M.D.; Benin, A.I.; Jakubczak, P.; Lanuza, M.; Galloway, D.B.; et al. Screening of Metal–Organic Frameworks for Carbon Dioxide Capture from Flue Gas Using a Combined Experimental and Modeling Approach. *J. Am. Chem. Soc.* **2009**, *131*, 18198–18199. [[CrossRef](#)] [[PubMed](#)]
15. Lee, S.C.; Chae, H.J.; Lee, S.J.; Park, Y.H.; Ryu, C.K.; Yi, C.K.; Kim, J.C. Novel regenerable potassium-based dry sorbents for CO₂ capture at low temperatures. *J. Mol. Catal. B Enzym.* **2009**, *56*, 179–184. [[CrossRef](#)]
16. Lee, S.C.; Choi, B.Y.; Lee, T.J.; Ryu, C.K.; Ahn, Y.S.; Kim, J.C. CO₂ absorption and regeneration of alkali metal-based solid sorbents. *Catal. Today* **2006**, *111*, 385–390. [[CrossRef](#)]

17. Lee, S.C.; Kim, J.C. Dry Potassium-Based Sorbents for CO₂ Capture. *Catal. Surv. Asia* **2007**, *11*, 171–185. [[CrossRef](#)]
18. Lee, S.C.; Kwon, Y.M.; Ryu, C.Y.; Chae, H.J.; Ragupathy, D.; Jung, S.Y.; Lee, J.B.; Ryu, C.K.; Kim, J.C. Development of new aluminium oxide-modified sorbents for CO₂ sorption and regeneration at temperatures below 200 °C. *Fuel* **2011**, *90*, 1465–1470. [[CrossRef](#)]
19. Plaza, M.G.; Pevida, C.; Arias, B.; Fermoso, J.; Rubiera, F.; Pis, J.J. A comparison of two methods for producing CO₂ capture adsorbents. *Energy Procedia* **2009**, *1*, 1107–1113. [[CrossRef](#)]
20. Przepiórski, J.; Skrodziewicz, M.; Morawski, A.W. High temperature ammonia treatment of activated carbon for enhancement of CO₂ adsorption. *Appl. Surf. Sci.* **2004**, *225*, 235–242. [[CrossRef](#)]
21. Lu, C.; Bai, H.; Wu, B.; Su, F.; Hwang, J.F. Comparative Study of CO₂ Capture by Carbon Nanotubes, Activated Carbons, and Zeolites. *Energy Fuels* **2008**, *22*, 3050–3056. [[CrossRef](#)]
22. Su, F.; Lu, C.; Cnen, W.; Bai, H.; Hwang, J.F. Capture of CO₂ from flue gas via multiwalled carbon nanotubes. *Sci. Total Environ.* **2009**, *407*, 3017–3023. [[CrossRef](#)] [[PubMed](#)]
23. Drage, T.C.; Arenillas, A.; Smith, K.M.; Pevida, C.; Piippo, S.; Snape, C.E. Preparation of carbon dioxide adsorbents from the chemical activation of urea–formaldehyde and melamine–formaldehyde resins. *Fuel* **2007**, *86*, 22–31. [[CrossRef](#)]
24. Jadhav, P.D.; Chatti, R.V.; Biniwale, R.B.; Labhsetwar, N.K.; Devotta, S.; Rayalu, S.S. Monoethanol Amine Modified Zeolite 13X for CO₂ Adsorption at Different Temperatures. *Energy Fuels* **2007**, *21*, 3555–3559. [[CrossRef](#)]
25. Su, F.; Lu, C.; Kuo, S.-C.; Zeng, W. Adsorption of CO₂ on Amine-Functionalized Y-Type Zeolites. *Energy Fuels* **2010**, *24*, 1441–1448. [[CrossRef](#)]
26. Lee, S.; Filburn, T.P.; Gray, M.; Park, J.-W.; Song, H.-J. Screening Test of Solid Amine Sorbents for CO₂ Capture. *Ind. Eng. Chem. Res.* **2008**, *47*, 7419–7423. [[CrossRef](#)]
27. Cho, E.-B.; Kim, D.; Mandal, M.; Gunathilake, C.A.; Jaroniec, M. Benzene-Silica with Hexagonal and Cubic Ordered Mesostructures Synthesized in the Presence of Block Copolymers and Weak Acid Catalysts. *J. Phys. Chem. C* **2012**, *116*, 16023–16029. [[CrossRef](#)]
28. Ma, X.; Wang, X.; Song, C. “Molecular Basket” Sorbents for Separation of CO₂ and H₂S from Various Gas Streams. *J. Am. Chem. Soc.* **2009**, *131*, 5777–5783. [[CrossRef](#)] [[PubMed](#)]
29. Yue, M.B.; Chun, Y.; Cao, Y.; Dong, X.; Zhu, J.H. CO₂ Capture by As-Prepared SBA-15 with an Occluded Organic Template. *Adv. Funct. Mater.* **2006**, *16*, 1717–1722. [[CrossRef](#)]
30. Hiyoshi, N.; Yogo, K.; Yashima, T. Adsorption characteristics of carbon dioxide on organically functionalized SBA-15. *Microporous Mesoporous Mater.* **2005**, *84*, 357–365. [[CrossRef](#)]
31. Knowles, G.P.; Delaney, S.W.; Chaffee, A.L. Diethylenetriamine[propyl(silyl)]-Functionalized (DT) Mesoporous Silicas as CO₂ Adsorbents. *Ind. Eng. Chem. Res.* **2006**, *45*, 2626–2633. [[CrossRef](#)]
32. Norihito, H.; Katsunori, Y.; Tatsuaki, Y. Adsorption of Carbon Dioxide on Amine Modified SBA-15 in the Presence of Water Vapor. *Chem. Lett.* **2004**, *33*, 510–511.
33. Plaza, M.G.; Pevida, C.; Arias, B.; Fermoso, J.; Arenillas, A.; Rubiera, F.; Pis, J.J. Application of thermogravimetric analysis to the evaluation of aminated solid sorbents for CO₂ capture. *J. Therm. Anal. Calorim.* **2008**, *92*, 601–606. [[CrossRef](#)]
34. Liu, X.; Li, J.; Zhou, L.; Huang, D.; Zhou, Y. Adsorption of CO₂, CH₄ and N₂ on ordered mesoporous silica molecular sieve. *Chem. Phys. Lett.* **2005**, *415*, 198–201. [[CrossRef](#)]
35. He, Y.; Seaton, N.A. Heats of Adsorption and Adsorption Heterogeneity for Methane, Ethane, and Carbon Dioxide in MCM-41. *Langmuir* **2006**, *22*, 1150–1155. [[CrossRef](#)] [[PubMed](#)]
36. Choi, S.; Drese, J.H.; Eisenberger, P.M.; Jones, C.W. Application of Amine-Tethered Solid Sorbents for Direct CO₂ Capture from the Ambient Air. *Environ. Sci. Technol.* **2011**, *45*, 2420–2427. [[CrossRef](#)] [[PubMed](#)]
37. Drese, J.H.; Choi, S.; Lively, R.P.; Koros, W.J.; Fauth, D.J.; Gray, M.L.; Jones, C.W. Synthesis–Structure–Property Relationships for Hyperbranched Aminosilica CO₂ Adsorbents. *Adv. Funct. Mater.* **2009**, *19*, 3821–3832. [[CrossRef](#)]
38. Sayari, A.; Belmabkhout, Y. Stabilization of Amine-Containing CO₂ Adsorbents: Dramatic Effect of Water Vapor. *J. Am. Chem. Soc.* **2010**, *132*, 6312–6314. [[CrossRef](#)] [[PubMed](#)]
39. Zelenák, V.; Badaničová, M.; Halamová, D.; Čejka, J.; Zukal, A.; Murafa, N.; Goerigk, G. Amine-modified ordered mesoporous silica: Effect of pore size on carbon dioxide capture. *Chem. Eng. J.* **2008**, *144*, 336–342. [[CrossRef](#)]

40. Zelenak, V.; Halamova, D.; Gaberova, L.; Bloch, E.; Llewellyn, P. Amine-modified SBA-12 mesoporous silica for carbon dioxide capture: Effect of amine basicity on sorption properties. *Microporous Mesoporous Mater.* **2008**, *116*, 358–364. [[CrossRef](#)]
41. Burkett, S.L.; Sims, S.D.; Mann, S. Synthesis of hybrid inorganic–organic mesoporous silica by co-condensation of siloxane and organosiloxane precursors. *Chem. Commun.* **1996**, *11*, 1367–1368. [[CrossRef](#)]
42. Macquarrie, D.J. Direct preparation of organically modified MCM-type materials. Preparation and characterisation of aminopropyl–MCM and 2-cyanoethyl–MCM. *Chem. Commun.* **1996**, *16*, 1961–1962. [[CrossRef](#)]
43. Harlick, P.J.E.; Sayari, A. Applications of Pore-Expanded Mesoporous Silicas. 3. Triamine Silane Grafting for Enhanced CO₂ Adsorption. *Ind. Eng. Chem. Res.* **2006**, *45*, 3248–3255. [[CrossRef](#)]
44. Knowles, G.P.; Graham, J.V.; Delaney, S.W.; Chaffee, A.L. Aminopropyl-functionalized mesoporous silicas as CO₂ adsorbents. *Fuel Process. Technol.* **2005**, *86*, 1435–1448. [[CrossRef](#)]
45. Mao, C.-F.; Vannice, M.A. High surface area α -aluminium oxide. I: Adsorption properties and heats of adsorption of carbon monoxide, carbon dioxide, and ethylene. *Appl. Catal. A General* **1994**, *111*, 151–173. [[CrossRef](#)]
46. Yong, Z.; Mata, V.; Rodrigues, A.E. Adsorption of Carbon Dioxide on Basic Aluminium oxide at High Temperatures. *J. Chem. Eng. Data* **2000**, *45*, 1093–1095. [[CrossRef](#)]
47. Chaikittisilp, W.; Kim, H.-J.; Jones, C.W. Mesoporous Aluminium Oxide-Supported Amines as Potential Steam-Stable Adsorbents for Capturing CO₂ from Simulated Flue Gas and Ambient Air. *Energy Fuels* **2011**, *25*, 5528–5537. [[CrossRef](#)]
48. Jeon, H.; Ahn, S.H.; Kim, J.H.; Min, Y.J.; Lee, K.B. Templated synthesis of mesoporous aluminium oxides by graft copolymer and their CO₂ adsorption capacities. *J. Mater. Sci.* **2011**, *46*, 4020–4025. [[CrossRef](#)]
49. Li, L.; Wen, X.; Fu, X.; Wang, F.; Zhao, N.; Xiao, F.; Wei, W.; Sun, Y. MgO/Al₂O₃ Sorbent for CO₂ Capture. *Energy Fuels* **2010**, *24*, 5773–5780. [[CrossRef](#)]
50. Gunathilake, C.; Gangoda, M.; Jaroniec, M. Mesoporous isocyanurate-containing organosilica–aluminium oxide composites and their thermal treatment in nitrogen for carbon dioxide sorption at elevated temperatures. *J. Mater. Chem. A* **2013**, *1*, 8244–8252. [[CrossRef](#)]
51. Asefa, T.; MacLachlan, M.J.; Coombs, N.; Ozin, G.A. Periodic mesoporous organosilicas with organic groups inside the channel walls. *Nature* **1999**, *402*, 867. [[CrossRef](#)]
52. Cai, W.; Yu, J.; Anand, C.; Vinu, A.; Jaroniec, M. Facile Synthesis of Ordered Mesoporous Aluminium Oxide and Aluminium Oxide-Supported Metal Oxides with Tailored Adsorption and Framework Properties. *Chem. Mater.* **2011**, *23*, 1147–1157. [[CrossRef](#)]
53. Kruk, M.; Jaroniec, M.; Sayari, A. Application of Large Pore MCM-41 Molecular Sieves to Improve Pore Size Analysis Using Nitrogen Adsorption Measurements. *Langmuir* **1997**, *13*, 6267–6273. [[CrossRef](#)]
54. Morris, S.M.; Fulvio, P.F.; Jaroniec, M. Ordered Mesoporous Alumina-Supported Metal Oxides. *J. Am. Chem. Soc.* **2008**, *130*, 15210–15216. [[CrossRef](#)] [[PubMed](#)]
55. Kumar, A.; Hua, C.; Madden, D.G.; O’Nolan, D.; Chen, K.-J.; Keane, L.-A.J.; Perry, J.J.; Zaworotko, M.J. Hybrid ultramicroporous materials (HUMs) with enhanced stability and trace carbon capture performance. *Chem. Commun.* **2017**, *53*, 5946–5949. [[CrossRef](#)] [[PubMed](#)]
56. Wickramaratne, N.P.; Jaroniec, M. Importance of small micropores in CO₂ capture by phenolic resin-based activated carbon spheres. *J. Mater. Chem. A* **2013**, *1*, 112–116. [[CrossRef](#)]
57. Bromberg, L.; Su, X.; Hatton, T.A. Aldehyde Self-Condensation Catalysis by Aluminum Aminoterephthalate Metal–Organic Frameworks Modified with Aluminum Isopropoxide. *Chem. Mater.* **2013**, *25*, 1636–1642. [[CrossRef](#)]
58. Gunathilake, C.; Jaroniec, M. Mesoporous alumina–zirconia–organosilica composites for CO₂ capture at ambient and elevated temperatures. *J. Mater. Chem. A* **2015**, *3*, 2707–2716. [[CrossRef](#)]
59. Gunathilake, C.; Dassanayake, R.S.; Abidi, N.; Jaroniec, M. Amidoxime-functionalized microcrystalline cellulose–mesoporous silica composites for carbon dioxide sorption at elevated temperatures. *J. Mater. Chem. A* **2016**, *4*, 4808–4819. [[CrossRef](#)]
60. Hanif, A.; Dasgupta, S.; Nanoti, A. High temperature CO₂ adsorption by mesoporous silica supported magnesium aluminum mixed oxide. *Chem. Eng. J.* **2015**, *280*, 703–710. [[CrossRef](#)]

61. Granados-Correa, F.; Bonifacio-Martinez, J.; Hernandez-Mendoza, H.; Bulbulian, S. Capture of CO₂ on gamma-Al₂O₃ materials prepared by solution-combustion and ball-milling processes. *J. Air Waste Manag. Assoc.* **2016**, *66*, 643–654. [[CrossRef](#)] [[PubMed](#)]
62. Thote, J.A.; Chatti, R.V.; Iyer, K.S.; Kumar, V.; Valechha, A.N.; Labhsetwar, N.K.; Biniwale, R.B.; Yenkie, M.K.; Rayalu, S.S. N-doped mesoporous alumina for adsorption of carbon dioxide. *J. Environ. Sci.* **2012**, *24*, 1979–1984. [[CrossRef](#)]
63. Wang, J.; Mei, X.; Huang, L.; Zheng, Q.; Qiao, Y.; Zang, K.; Mao, S.; Yang, R.; Zhang, Z.; Gao, Y.; et al. Synthesis of layered double hydroxides/graphene oxide nanocomposite as a novel high-temperature CO₂ adsorbent. *J. Energy Chem.* **2015**, *24*, 127–137. [[CrossRef](#)]



© 2018 by the authors. Licensee MDPI, Basel, Switzerland. This article is an open access article distributed under the terms and conditions of the Creative Commons Attribution (CC BY) license (<http://creativecommons.org/licenses/by/4.0/>).